AIChE

A General Procedure for Obtaining the Evolving Particle-Size Distribution of Flocculating Suspensions

Y. Leong Yeow
Dept. of Chemical and Biomolecular Engineering, The University of Melbourne, Victoria 3010, Australia

Jong-Leng Liow
School of Engineering and Information Technology, Australian Defence Force Academy, The University of New South Wales, Canberra ACT 2600, Australia

Yee-Kwong Leong
School of Mechanical Engineering, University of Western Australia, Crawley, Western Australia 6009, Australia

DOI 10.1002/aic.13710
Published online December 14, 2011 in Wiley Online Library (wileyonlinelibrary.com).

A numerical procedure has been developed to solve the population balance equation (PBE) for the flocculation of colloidal suspensions. It has the flexibility to cope with different flocculation kinetics and spread in particle volume. The two key steps in this procedure are the adoption of the logarithm of particle volume as the independent variable and the implementation of uniform discretization in the logarithmic domain. Together they allow the PBE to be represented accurately over the entire particle range overcoming the failure of the popular geometric discretization scheme to represent the PBE satisfactorily for large particles. The Method of Lines is used to convert the PBE from an integro-differential equation into a set of first-order ordinary differential equations, which is then integrated using commercial scientific computing software. The procedure has been tested for different kinetics and initial particle distributions. Preservation of particulate volume of between 1 and 8% is consistently observed. © 2011 American Institute of Chemical Engineers *AIChE J,* 58: 3043–3053, 2012
Keywords: flocculation, particulate processes, particle-size distribution, integro-differential equation, Method of Lines

Introduction

Particle-size distribution (PSD) is a key variable in industrially important particulate processes such as fine particle production by grinding, drop size control in solvent extraction and in cell aggregation, and flocculation of colloidal particles of various suspensions.[1,2] It describes the temporal evolution of particulate composition from the initial state toward the final equilibrium state. PSD takes the form of a curve that relates the number concentration density function $n(t, v)$ to time t and particle size v. At any t, $\delta n = n(t, v)\delta v$ gives the number concentration δn of particles with volume between $v - \delta v/2 < v < v + \delta v/2$ and $v \times n(t, v)\delta v$ gives the volume occupied by particles in this size range. $n(t, v)$ is assumed to be a well-behaved function of the two independent variables t and v.

In a typical particulate process, large particles are continuously being formed by agglomeration of smaller ones and at the same time small particles are being generated by fragmentation of larger ones. For any particle size v, the imbalance between agglomeration and fragmentation shows up as the growth or decay of its number concentration density function $(\partial n/\partial t)_v$. An explicit expression for $(\partial n/\partial t)_v$ over the entire size range observed in a particulate process can be obtained by balancing the agglomeration and fragmentation rates. This equation is now generally referred to as the population balance equation (PBE).[1,2] In the derivation of this equation, a number of assumptions are made regarding the kinetics of agglomeration and fragmentation. To keep the presentation reasonably self-contained and to introduce the notations used, the kinetic expressions will be introduced in the next section for the specific case of flocculation. As most of the underlying assumptions are generally valid for other particulate processes, the results obtained here together with their physical significance and the solution procedure are, with minimal modifications, also valid for these other particulate processes. The main aim of this presentation is to describe a numerical method for solving the PBE for $n(t, v)$, which can be regarded as a further development of the method described by Yeow et al. for solving the temporal evolution of molecular weight distribution in the thermal disintegration of macromolecules in which only fragmentation is observed.[3] However, the simultaneous presence of aggregation and fragmentation together with the much larger range of particle volume involved, compared with that of molecular weight, means that a significant number of new problems are encountered that require major modifications of the numerical solution procedure.

Correspondence concerning this article should be addressed to Y. Leong Yeow at yly@unimelb.edu.au.

Agglomeration and Fragmentation Kinetics and the PBE

There is a very extensive literature on the kinetics of particle agglomeration and of fragmentation.[4–7] It covers the

physical origin of the forces responsible for these two fundamental processes and the variation of their rates with particle size and with the chemical and physical properties of the suspending fluid. It also considers the effects of the kinematics of the suspending fluid, particularly that of turbulence, on these rates. For the purpose of developing a general method for obtaining the evolving PSD curves, instead of dealing with the large number of specific cases, it will be more fruitful to test the performance of the method on relatively simple yet general kinetic models that reflect most of the experimentally observed behavior. Special attention will be taken to ensure that the solution method has the necessary flexibility to cope with the more complex kinetic features suggested by empirical data or theoretical considerations. It is also essential that the method can handle most initial PSD data and follow its evolution toward the final equilibrium state.

Kinetics of agglomeration

In most flocculation investigation, the rate of formation r_A of a large particle v_u by the agglomeration of two smaller ones v_s and v_t

$$v_s + v_t \rightarrow v_u \tag{1}$$

is assumed to depend on the number concentration density functions $n(t, v_s)$ and $n(t, v_t)$ of the two agglomerating species and follows second-order kinetics

$$r_A = k_A(v_s, v_t)n(t, v_s)n(t, v_t). \tag{2}$$

To allow for the effects of particle size on agglomeration rate, the usual rate constant is replaced by a rate function $k_A(v_s, v_t)$, which is taken to be an explicit function of the size of the two agglomerating particles. Following the common assumption of flocculation investigations, agglomeration is assumed to be isochoric, that is, $v_u = v_s + v_t$. Thus, the effects of v_u on r_A are implicitly allowed for in Eq. 2. Through suitable choice of the functional form of $k_A(v_s, v_t)$, most agglomeration kinetics discussed in the literature can be accommodated by this function.[4–6]

Kinetics of fragmentation

The fragmentation of a large particle v_r into two smaller product particles v_p and v_q

$$v_r \rightarrow v_p + v_q \tag{3}$$

is generally assumed to be a first-order process in which the rate of fragmentation r_F is given by a kinetic expression of the form

$$r_F = k_F(v_r, v_p)n(t, v_r). \tag{4}$$

As in agglomeration, to allow for the dependence of r_F on particle size v_r and on product size v_p, Eq. 4 has a first-order rate function $k_F(v_r, v_p)$ instead of a first-order rate constant. Following the notation adopted by Yeow et al., only v_r and v_p appear explicitly in this rate function. The dependence on v_q is implicit as $v_q = v_r - v_p$ for isochoric fragmentation.[3] Starting from a few simple but physically realistic assumptions, it is possible to construct $k_F(v_r, v_p)$'s that reflect most of the experimentally reported fragmentation behavior.[5–7]

Population balance equation

The equation governing the evolution of PSD, that is, $\partial n(t, v)/\partial t$ with v held fixed can be obtained by balancing the rate of generation of particles with size v against that for its disappearance. Based on the general rate expressions in Eqs. 2 and 4, such a balance leads directly to

$$\begin{aligned}\frac{\partial n(t,v)}{\partial t} = &\frac{1}{2}\int_{v_s=v_{\min}}^{v-v_{\min}} k_A(v_s, v-v_s)n(t,v_s)n(t,v-v_s)dv_s \\ &- n(t,v)\int_{v_t=v_{\min}}^{v_{\max}-v} k_A(v,v_t)n(t,v_t)dv_t \\ &+ \int_{v_r=v+v_{\min}}^{v_{\max}} k_F(v_r,v)n(t,v_r)dv_r \\ &- \frac{1}{2}n(t,v)\int_{v_p=v_{\min}}^{v-v_{\min}} k_F(v,v_p)dv_p \end{aligned} \tag{5}$$

where $v_{\max}$ and $v_{\min}$ are, respectively, the largest and the smallest particle size encountered in a flocculation process. The first integral on the righthand side (RHS) gives the rate of generation of v particles as a result of the agglomeration of particles v_s with $v - v_s$ for v_s in the range $v_{\min}$ to $v - v_{\min}$. The second integral gives the rate of disappearance of v particles as a result of the agglomeration of such a particle with a particle v_t in the range $v_{\min}$ to $v_{\max} - v$ in the flocculating suspension. The third integral gives the rate of generation of v particles arising from the fragmentation of all particles $v_r \geq v + v_{\min}$ into a v particle and a second particle $v_r - v$. The final integral accounts for the rate of disappearance of size v particles as a result of their fragmentation into all possible combinations of two smaller particles v_p and $v - v_p$, where $v_{\min} \leq v_p \leq v - v_{\min}$.

Apart from differences in notation, Eq. 5 is the PBE adopted by most investigators of flocculation.[8–10] The various limits of the four integrals are based on physical considerations that are essentially self-explanatory with the possible exception of the upper limit in the second integral. The limit there is $v_{\max} - v$ instead of $v_{\max}$ or infinity as frequently encountered in the literature. This upper limit ensures that particles larger than $v_{\max}$ are not generated by agglomeration so as to be consistent with the assumption that $v_{\max}$ is the largest observed particle size in the flocculation process under investigation. In some variants of the PBE, the lower limit for the first, second, and fourth integrals are taken to be 0. Zero particle volume cannot be accommodated by the logarithmic-independent variable introduced below and is also physically unrealistic.

The numerical factor of 1/2 in the first and fourth integrals in Eq. 5 is there to compensate for the double counting of the rate of generation by the first integral and the rate of disappearance by the fourth integral.

In the derivation of the PBE, it is assumed that there is no creation or disappearance of particulates, for example, through nucleation followed by growth or dissolution of particulates. This coupled with the isochoric assumption means that the total volume of particulates per unit volume of the suspension remains constant throughout the flocculation process. This volume, denoted by m_F, is given by $m_F = \int_{v=v_{\min}}^{v_{\max}} vn(t,v)dv$, which is mathematically referred to as the first moment of the PSD. A closely related quantity is the zeroth moment $m_Z(t)$ defined by $m_Z(t) = \int_{v=v_{\min}}^{v_{\max}} n(t,v)dv$.

This gives the number of particles per unit volume of the suspension. As particles aggregate and disintegrate $m_Z(t)$ will in general either increase or decrease with time.

Dimensionless and Logarithmic Variables and Equations

To keep the computation steps general and to simplify the presentation of numerical results, the procedure developed below solves the PBE in dimensionless form. Equation (5) is made dimensionless by the introduction of the following dimensionless variables and kinetic functions: $V = v/v_{\max}$, $N = (v_{\max})^2\, n/m_F$, $K_F = k_F/k_{F\max}$, $K_A = k_A m_F/(v_{\max}{}^2 k_{F\max})$, $\tau = t \times v_{\max} k_{F\max}$. For simplicity, the dependence of the dimensionless-dependent variable and kinetic functions on dimensionless time τ and dimensionless particle volume V has been suppressed in these defining expressions. As implied by its subscript, the scaling factors $k_{F\max}$ is the maximum value of the fragmentation kinetic function over all possible combinations of v_r and v_p encountered in the flocculation process under investigation. From the definition of $N(\tau, V)$ and m_F, it follows that the dimensionless first moment $M_F \equiv \int_{V=V_{\min}}^{1} VN(\tau,V)dV$ takes on the value of unity.

The dimensionless PBE takes the form

$$\frac{\partial N(\tau,V)}{\partial \tau} = \frac{1}{2}\int_{V_s=V_{\min}}^{V-V_{\min}} K_A(V_s, V-V_s)N(\tau,V_s)N(\tau,V-V_s)dV_s - N(\tau,V)\int_{V_t=V_{\min}}^{V_{\max}-V} K_A(V,V_t)N(\tau,V_t)dV_t + \int_{V_r=V+V_{\min}}^{V_{\max}} K_F(V_r,V)N(\tau,V_r)dV_r - \frac{1}{2}N(\tau,V)\int_{V_p=V_{\min}}^{V-V_{\min}} K_F(V,V_p)dV_p. \quad (6)$$

The general form of the dimensionless agglomeration kinetic function in Eq. 6 to be used in the examples below is

$$K_A(V_s,V_t) = \kappa_A \exp[\lambda(V_s)^a]\exp[\lambda(V_t)^a]\exp[\eta(V_s+V_t)^b]. \quad (7)$$

The physical significance of the parameters in this expression is simple to observe. κ_A, a positive constant, controls directly the magnitude of the agglomeration function. The exponents a and b change the way particle size affects the aggregation rate. Guided by the empirical assumptions in the literature, a and b usually take on values of either ± 1 or $\pm 1/3$. The former implies that the rate is controlled by particle volume and the latter suggests that it is the equivalent diameter that is in direct control. The parameters λ and η set the sensitivity of the rate function to changing particle size. Figure 1 shows examples of the variation of K_A for some typical combinations of these parameters. In these plots V_s, on the horizontal axis, varies from $V_{\min}$ to 1 and V_t, as a parameter, is kept fixed at selected values between these limits on each individual curve. It is clear that the aggregation rate can exhibit quite different behavior with the small number of parameter combinations shown here.

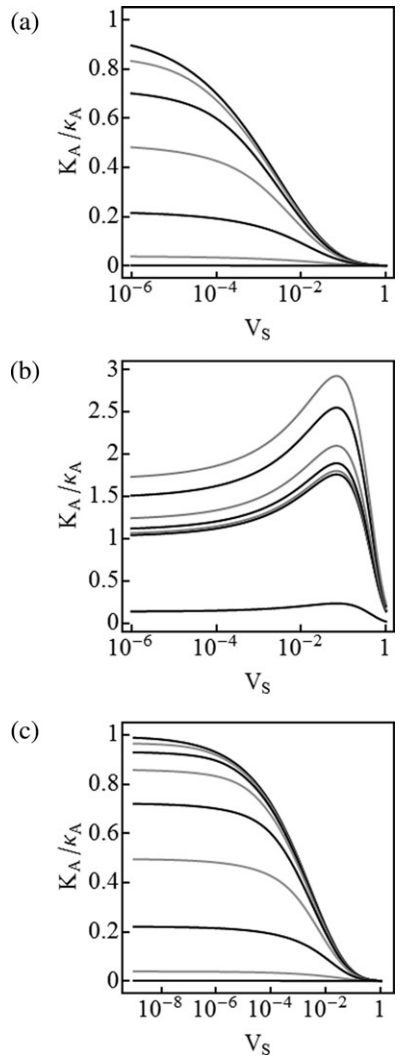

Figure 1. Aggregation kinetics based on Eq. 2.

(a) $a = b = 1/3$, $\lambda = -3$, $\eta = -4$, $V_{\min} = 10^{-6}$ and $V_t = 10^{-6}$ (top most), 10^{-5}, 10^{-4}, 10^{-3}, 0.01, 0.1, 1 (lowest); (b) $a = 1/3$, $b = 1$, $\lambda = 2$, $\eta = -4$, $V_{\min} = 10^{-6}$ and $V_t = 10^{-1}$ (top most), 10^{-2}, 10^{-3}, 10^{-4}, 10^{-5}, 10^{-6}, 1 (lowest); (c) $a = b = 1/3$, $\lambda = -3$, $\eta = -4$, $V_{\min} = 10^{-9}$ and $V_t = 10^{-9}$ (top most), 10^{-7}, 10^{-6}, 10^{-5}, 10^{-4}, 10^{-3}, 0.01, 0.1, 1 (lowest).

The corresponding dimensionless fragmentation kinetic function in Eq. 6 has the general form

$$K_F(V_r,V_p) = \frac{\exp[\sigma(V_r)^g](V_p - V_{\min})^h (V_r - V_p - V_{\min})^h}{\exp(\sigma)(V_r/2 - V_{\min})^{2h}}. \quad (8)$$

This is a modification of the kinetic function adopted by Yeow et al.[3] It is based on the plausible assumption that in binary fission the fragmenting particle is more likely to disintegrate into two particles of approximately the same size than two of vastly different sizes.[7] The exponents g and h play the same role as a and b in Eq. 7. σ, assumed to be positive, controls how the fragmentation rate increases with the size of the fragmenting particle. The factors in the denominator ensure that $\mathrm{Max}[K_F] = 1$ as defined. Typical plots of $K_F(V_r, V_p)$ against V_r are shown in Figure 2. V_p appears as a parameter that is held fixed on each curve. All the plots are for $V_{\min} = 10^{-6}$ but the general shape of the curves is not affected greatly by changes in $V_{\min}$. Again, vastly different behavior in $K_F(V_r, V_p)$ besides those shown in Figure 2 can be simulated by Eq. 8.

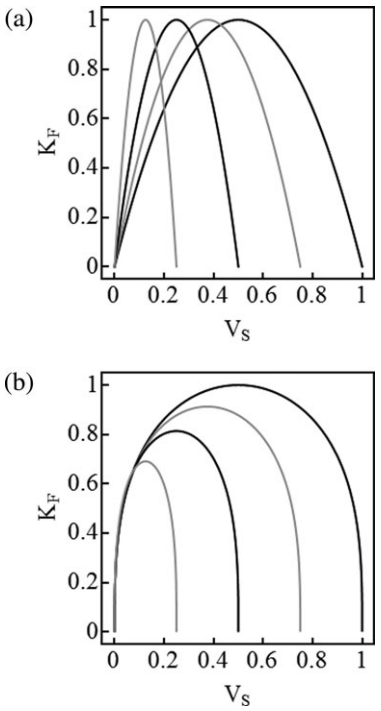

Figure 2. Fragmentation kinetics based on Eq. 4.

(a) $g = h = 1$, $\sigma = 0$, $V_{min} = 10^{-6}$ (or 10^{-9}), $V_p = 0.25$ (left most), 0.5, 0.75, 1 (rightmost); (b) $g = h = 1/3$, $\sigma = 1$, $V_{min} = 10^{-6}$, $V_p = 0.25$ (left most), 0.5, 0.75, 1 (rightmost).

In a typical flocculation operation, the smallest and the largest particle size, in terms of equivalent spherical diameter, can differ by 2–3 orders of magnitude. For example, the smallest diameter can be around 1 μm and the largest can be as large as 1 mm.[10] In terms of particle volume, this represents a spread of between 6 and 9 decades, that is, V_{min} as defined above is likely to be between 10^{-9} and 10^{-6}. To present experimental PSD over such a large spread in particle volume, it is normal practice to replace V by $X = \log_{10} V$ as the independent variable with X_{min} varying between -9 and -6.

Making the direct substitution $dV = \log_e 10 \times 10^X dX$, the transformed PBE takes the form

$$\frac{\partial N(\tau, 10^X)}{\partial \tau} = \frac{1}{2}\int_{X_s=X_{min}}^{X\leftrightarrow X_{min}} K_A(10^{X_s}, 10^{X\leftrightarrow X_s}) N\left(\tau, 10^{X_s}\right) \times N(\tau, 10^{X\leftrightarrow X_s}) 10^{X_s} \log_e 10\, dX_s - N\left(\tau, 10^X\right) \int_{X_t=X_{min}}^{X_{max}\leftrightarrow X} K_A(10^X, 10^{X_t}) N\left(\tau, 10^{X_t}\right) 10^{X_t} \log_e 10\, dX_t + \int_{X_r=X\oplus X_{min}}^{X_{max}} K_F(10^{X_r}, 10^X) N\left(\tau, 10^{X_r}\right) 10^{X_r} \log_e 10\, dX_r - \frac{1}{2} N\left(\tau, 10^X\right) \int_{X_p=X_{min}}^{X\leftrightarrow X_{min}} K_F(10^X, 10^{X_p}) 10^{X_p} \log_e 10\, dX_p. \quad (9)$$

In this equation, the dependent variable $N(\tau, V)$ and the assumed kinetic functions $K_A(V_s, V_t)$ and $K_F(V_r, V_p)$, are now treated as functions of X. The limits of the integrals are also expressed in terms of X. Unlike physical variable V, the logarithmic variable X is not additive. This means that to obtain the X that corresponds to terms such as $V - V_{min}$ and $V + V_{min}$ in Eq. 6, they will have to be evaluated in the physical domain and then mapped onto the logarithmic domain. To keep Eq. 9 tidy, the following notations have been introduced.

$$X \leftrightarrow X_{min} \equiv \log_{10}(10^X - 10^{X_{min}}), X \leftrightarrow X_s \equiv \log_{10}(10^X - 10^{X_s}),$$
$$X_{max} \leftrightarrow X \equiv \log_{10}(1 - 10^X), X \oplus X_{min} \equiv \log_{10}(10^X + 10^{X_{min}}). \quad (10)$$

Nonstandard symbols $\leftrightarrow$ and $\oplus$ are used to emphasize that the differencing and summing operations were performed in the physical domain and then mapped on to the logarithmic domain.

In the numerical solution scheme, the interval $X_{min} \le X \le X_{max} = 0$ is discretized into N_D uniformly spaced discretization points. Depending on X_{min}, N_D is typically between 401and 1001. A uniform grid in X is able to provide a far more satisfactory representation of the PSD data that spread over 6–9 decades than a uniform grid in V. This is because, in a uniform grid in V, most of the discretization points will be located in the final (largest) decade of particle volume with fewer and fewer points per decade as V decreases. For example, if a uniform grid in V with $N_D = 1001$ is used to represent a PSD that spreads over 9 decades, that is, $V_{min} = 10^{-9}$ and $V_{max} = 1$, 900 of these points will be located in the final decade $0.1 \le V \le 1$, with 90 points in the next largest decade $0.01 \le V \le 0.1$ and only 11 points to cover the remaining interval between $10^{-9} \le V \le 0.01$. Such a grossly uneven distribution of discretization points clearly is unable to provide a workable description of the evolving PSD as it moves over several decades of particle volume. A uniform grid in X, by design, will ensure that the PSD is represented by the same number of discretization points over all the 9 decades. Thus, there will be 101 discretization points in each unit interval of X over the entire span of $-9 \le X \le 0$. This ensures that the PSD data are evenly and more adequately represented during the solution of the PBE.

Discretized Equations

Equation 9 is in the form of a nonlinear integro-differential equation for $N(\tau, V)$ with the kinetic functions, $K_A(V_r, V_p)$ and $K_F(V_s, V_t)$, regarded as known functions either based on theoretical considerations or deduced from experimental data. Although there does not appear to be a generally accepted procedure for dealing with integro-differential equations,[11,12] recently Yeow et al. demonstrated that Method of Lines (MoL)[13] provides a practical and workable means of solving the PBE of thermal fragmentation of macromolecules. There are earlier reports, some dating back 40–50 years before MoL became the accepted nomenclature, of similar treatment of the PBE. In this method, each of the integrals on the RHS of the integro-differential equation is approximated by numerical quadrature using the simple trapezoidal rule. This has the effect of converting the integro-differential equation into a set of simultaneous first-order ordinary differential equations (ODEs). These equations are then integrated using standard Runge–Kutta routine found in most commercial scientific computing software.[12] As a description of the implementation of this solution procedure

can be found in Yeow et al.,[3] the corresponding details for applying it to Eq. 9 will not be repeated here. Instead emphasis will be placed on the complications introduced by flocculation and similar particulate processes that are not present in thermal fragmentation of macromolecules. The additional numerical steps brought about by the logarithmic variable will also be described.

The span of the independent variable $X_{\min} \le X \le X_{\max} = 0$, divided into N_D uniformly spaced points, will be represented by the column vector $[X_1, X_2 \ldots X_i, \ldots X_{N_D}]^T$. In the discretized form, the unknown function $N(\tau, 10^X)$ is replaced by a set of N_D unknown functions, one at each discretization point X_i, of the dimensionless time τ—the remaining independent variable. This set of unknown functions will be denoted by the column vector

$$\mathbf{N}(\tau) = [N_1(\tau), N_2(\tau), \ldots N_i(\tau), \ldots N_{N_D}(\tau)]^T. \quad (11)$$

Substituting these into Eq. 9 and replacing the integrals by trapezoidal-rule approximation, the integro-differential equation leads directly to a set of N_D simultaneous first-order ODEs for the $N_i(\tau)$. These ODEs take the general form

$$\begin{aligned}\frac{dN_i}{d\tau} = {} & \frac{\log_e 10}{2}\left\{\sum_{s=1}^{i\leftrightarrow 1}\alpha_{is}K_{As,i\leftrightarrow s}\times 10^{X_s}N_sN_{i\leftrightarrow s}\right\}\Delta X \\ & - \log_e 10\left\{\sum_{t=1}^{N_{D\leftrightarrow i}}\beta_{it}K_{Ai,t}10^{X_t}N_t\right\}N_i\Delta X \\ & + \log_e 10\left\{\sum_{r=i\oplus 1}^{N}\chi_{ir}K_{Fr,i}10^{X_r}N_r\right\}\Delta X \\ & - \frac{\log_e 10}{2}\left\{\sum_{p=1}^{i\leftrightarrow 1}\gamma_{ip}K_{Fi,p}10^{X_p}\right\}N_i\Delta X \quad \text{for } i = 1 \text{ to } N_D\end{aligned} \quad (12)$$

$\Delta X = (X_{\max} - X_{\min})/(N_D - 1)$ is the uniform discretization step size in X and α_{is}, β_{it}, χ_{ir}, and γ_{ip} are known numerical coefficients arising from the approximation of the four integrals in Eq. 9 by the trapezoidal quadrature rule.

At all discretization points in the interior of the interval of any of the four integrals, the trapezoidal-rule coefficient takes the value of unity. If the upper or lower limit of an integral coincides with a discretization point, the coefficient there takes the usual end value of 1/2. For those differencing and summation limits in Eq. 12 that do not coincide with a grid point, the trapezoidal-rule coefficients are determined by linear interpolation of neighboring grid points. Similarly, unknown $N(\tau, V)$ at a nongrid point location that appears in Eq. 12 is expressed as linear combination of its two nearest neighbors in the column vector $\mathbf{N}(\tau)$. These are relatively minor complications and can be handled automatically by computer requiring only a minimal amount of additional programming effort. Other than these issues, the implementation of the MoL scheme using commercial software to solve the resulting set of ODEs follows closely the steps reported by Yeow et al.[3]

Results

The solution procedure based on MoL will now be used to obtain the evolving PSD for a number of simulated initial size distributions with width increasing from 6 to 9 decades in particle volume.

Initial data spreading over 6 decades and kinetics in Figures 1a and 2a

Laboratory PSD data of flocculating suspensions are not normally reported as $n(t, v)$ instead they are usually presented as volume fraction density function $G(\tau, X)$ as a function of $X \equiv \log_{10} V$. The discrete points in Figure 3a represent a set of simulated initial PSD data denoted by $G_{ini}(X)$ spreading over 6 decades of particle volume. The area of the vertical strip $G_{ini}(X)\delta X$ represents the volume, as a fraction of total particulate volume, occupied by particles in the size range $X - 1/2\delta X \le X \le X + 1/2\delta X$. $G_{ini}(X)$ has to be converted into the initial condition $N_{ini}(V)$ for the MoL procedure. From their definitions, $G_{ini}(X)$ and $n_{ini}(v)$ are related by the simple relationship $G_{ini}(X)\delta X = v \times n_{ini}(v)\delta v/m_F = V \times N_{ini}(V)\delta V$. From this it follows that

$$N_{ini}(10^X) = \frac{G_{ini}(X)}{\log_e 10 \times 10^{2X}}. \quad (13)$$

The $N_{ini}(V)$ or equivalently the $N_{ini}(10^X)$ derived from Figure 3a is shown as discrete points in Figure 3b where N_{max} is the maximum value of $N_{ini}(10^X)$. The converse of Eq. 13

$$G(\tau, X) = \log_e 10 \times 10^{2X} N(\tau, 10^X) \quad (14)$$

allows the evolving $N(\tau, V)$ generated by MoL to be converted back to volume fraction $G(\tau, X)$. Even though $N(\tau, V)$ and $G(\tau, X)$ describe the same PSD, their shapes are quite different and they complement one another in providing insight into the progress of the flocculation process. Both descriptions will be reported in this investigation.

Starting with the $N_{ini}(V)$ in Figure 3b and assuming the kinetic functions in Figure 1a with $\kappa_A = 50$ and Figure 2a, the evolving $N(\tau, V)$ given by the numerical solution of

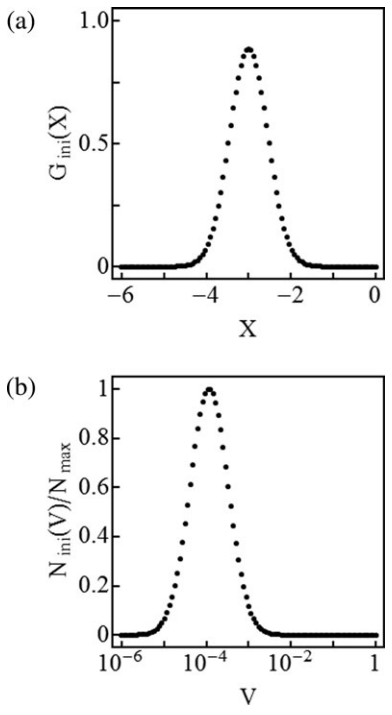

Figure 3. Simulated initial PSD.

(a) Plotted as $G_{ini}(X)$ spreading over $-6 \le X \le 0$; (b) replotted as $N_{ini}(V)/N_{max}$ spreading over $10^{-6} \le V \le 1$.

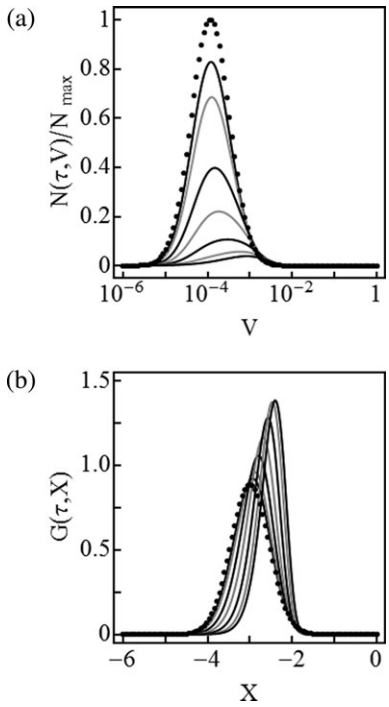

Figure 4. PSD curves of flocculation for the kinetics in Figures 1a and 2a with $V_{min} = 10^{-6}$ and $\kappa_A = 50$.

Plotted as $N(\tau, V)/N_{max}$ in (a) and as $G(\tau, V)$ in (b) for $\tau = 0$ (discrete points), 20, 40, 100, 200, 400, 800, and 5000. $\tau = 5000$ is the lowest curve in (a) and the rightmost curve in (b).

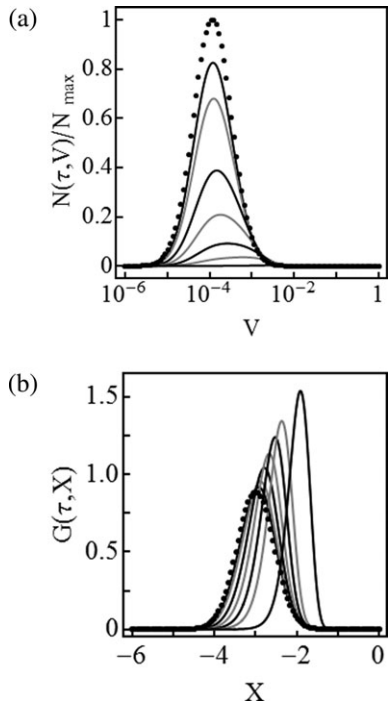

Figure 5. PSD curves of aggregation for the kinetics in Figure 1a with $V_{min} = 10^{-6}$ and $\kappa_A = 50$.

Plotted as $N(\tau, V)/N_{max}$ in (a) and $G(\tau, V)$ in (b) for the same set of τ in Figure 4. $\tau = 5000$ is the lowest curve in (a) and the rightmost curve in (b).

Eq. 12 is shown as continuous curves in Figure 4a. The corresponding $G(\tau, X)$ is shown in Figure 4b. The different curves are for the dimensionless time τ shown in the figure caption. These τ values were chosen to space out the PSD curves. The discrete points in these plots represent the initial distribution. The gradual reduction in height of the curves in Figure 4a and the gradual shift of the curves to the right in Figure 4b indicate that agglomeration is proceeding faster than fragmentation. The trends of these curves indicate that the flocculation process is slowing down and is approaching the equilibrium state at around $\tau = 5000$.

It is interesting to examine the corresponding PSD when the particles only undergo aggregation and only undergo fragmentation. These are readily obtained by switching off the fragmentation terms or the aggregation terms in Eq. 12. The resulting PSD curves are shown in Figure 5 for aggregation and in Figure 6 for fragmentation. Large particles at low concentration formed by the aggregation process that do not show up in the $N(\tau, V)$ plots show up clearly in the $G(\tau, X)$ plots (see Figures 5a, b). Conversely, the presence of small particles generated by fragmentation that does not shows up in the $G(\tau, X)$ plots can be seen in the $N(\tau, V)$ plots. This is particularly clear when comparing Figures 6a, b. The temporal trends of the curves in Figures 5 and 6, compared with that of Figure 4, are consistent with the expected behavior of purely agglomerating and purely fragmenting system, respectively.

In arriving at the results in Figures 4–6, the number of discretization points N_D is 801. Particulate volume preservation has been checked by evaluating the first moment M_F of the computed $N(\tau, V)$ curves or equivalently the area under the $G(\tau, X)$ curves. The maximum deviation of M_F from unity is around 1%. This is generally observed at large τ in the PSD of flocculation or aggregation. This is attributed to the accumulation of error during the integration of the ODEs. The small deviation of M_F can be regarded as an indication of the level of accuracy of the computed PSD.

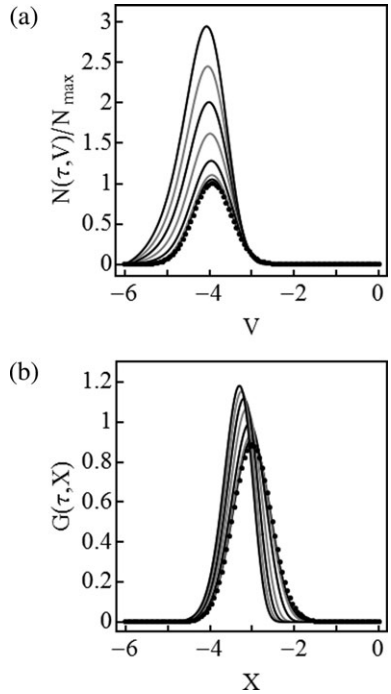

Figure 6. PSD curves of fragmentation for the kinetics in Figure 2a with $V_{min} = 10^{-6}$.

Plotted as $N(\tau, V)/N_{max}$ in (a) and $G(\tau, V)$ in (b) for the same set of τ in Figure 4. Curves move from right to left in both plots.

Particulate volume preservation check will be performed for all the results presented below and unless otherwise stated deviation is below 10% and for most cases well below 5%. This is achieved by, where necessary, increasing the number of discretization points N_D from a low of 401 to as high as 1001.

Initial data of Figure 3 and kinetics in Figures 1b and 2b

The computed PSD curves using the agglomeration kinetics in Figure 1b with $\kappa_A = 50$ and the fragmentation kinetics in Figure 2b are shown in Figure 7. The initial condition is that in Figure 3a. $N_D = 1001$ in these results.

It is interesting to compare, albeit only qualitatively, the PSD curves of this example with that of the previous example. The PSD curves in Figure 7, particularly those in Figure 7b show that, at around $\tau = 1000$, the flocculation process is approaching equilibrium. Compared with curves in Figure 4, equilibrium in this case is attained at a smaller τ. Furthermore, the equilibrium PSD in Figure 7b has shifted further to the right than that in Figure 4b. This is likely to be a consequence of the generally larger $K_A(V_s, V_t)$ in Figure 1b compared with that in Figure 1a. Similar comparison of the PSD curves for pure aggregation and pure fragmentation (not shown) for the kinetic functions of this example with those in Figures 5 and 6 also suggests that their differences are consistent with the differences in the kinetics of these two cases.

To keep particulate volume preservation at approximately the same level as that in Figures 4–6, it was necessary to use a higher N_D of 1001 for the results in Figure 7. This is attributed to the general steeper gradient of the fragmentation and aggregation kinetic curves of this example compared with that of the previous example.

Initial data of Figure 8 and kinetics of Figures 1c and 2a

This example considers the performance of the logarithmic variable X in dealing with PSD that spreads over 9 decades in particle volume. The simulated initial data for this example are shown as discrete points in Figure 8. The aggregation kinetics assumed is that shown in Figure 1c again with $\kappa_A = 50$ and the corresponding fragmentation kinetics is again that shown in Figure 2a but with $V_{min} = 10^{-9}$. Following the presentation format of previous examples, the resulting PSD generated by Eq. 12 is shown as continuous $N(\tau, V)$ and $G(\tau, X)$ curves in Figure 8. The presence of small particles shows up clearly in the $N(\tau, V)$ plot and that of larger ones in the $G(\tau, X)$ plot. $N_D = 1001$ was used in these results and M_F deviated from unity by approximately 8%. This increased deviation of M_F is a consequence of the reduced number of discretization points per decade. The choice of N_D here is a balance between keeping M_F close to unity and maintaining an acceptable computing time. At the largest dimensionless time $\tau = 10{,}000$ shown in Figure 8, the flocculation process has not attained equilibrium. The $G(\tau, X)$ curves in Figure 8b shows that aggregation of small particles, which moves the PSD to larger sizes, is counteracted by fragmentation of the larger particles, which moves the PSD back to smaller sizes.

As a result, the $G(\tau, X)$ curves exhibit a narrowing base and a sharpening peak centered around $V = 10^{-4}$. To reduce the deviation of M_F will require either further increase in N_D or alternatively solving the PBE numerically for a reduced range of V restricting it to the region where $N(\tau, V)$ and $G(\tau, X)$ are significant. The former will push the computing problem beyond the resources of the current generation of laptop computers. The latter is conditional on the existence

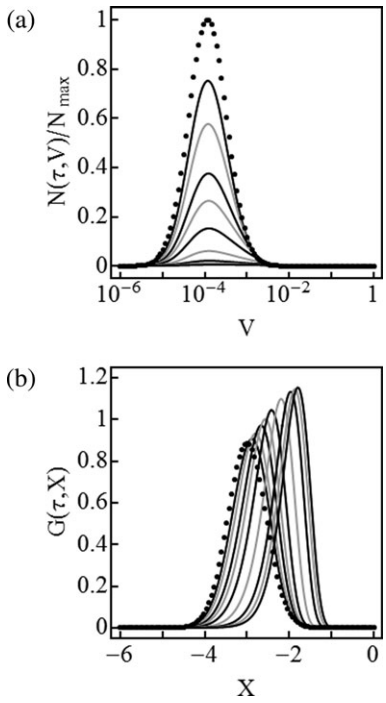

Figure 7. PSD of fragmentation for the kinetics in Figures 1b and 2b with $V_{min} = 10^{-6}$ and $\kappa_A = 50$.

Plotted as $N(\tau, V)/N_{max}$ in (a) and replotted as $G(\tau, X)$ in (b) for $\tau = 0$ (discrete points), 10, 20, 40, 60, 100, 200, 400, 600, and 1000. $\tau = 1000$ is the lowest curve in (a) and the rightmost in (b).

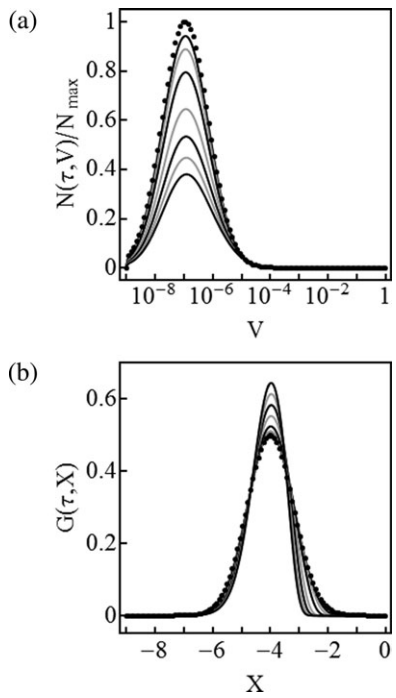

Figure 8. PSD curves of flocculation for the kinetics in Figures 1c and 2a with $V_{min} = 10^{-9}$ and $\kappa_A = 50$.

Plotted as $N(\tau, V)/N_{max}$ in (a) and $G(\tau, X)$ in (b). $\tau = 0$ (discrete points), 500, 1000, 2000, 4000, 6000, 8000, and10,000. $\tau = 10{,}000$ is the lowest curve in (a) and the tallest curve in (b).

of a lower subset and/or an upper subset of particle size over which both $N(\tau, V)$ and $G(\tau, X)$ are negligible. Depending on the combination of initial condition and kinetics, such subsets may not exist or if they exist they may be so small that it would not improve the resolution problem significantly. Both of these possible approaches have not been explored.

Comparison with exact solution of droplet coalescence

Scott[14] investigated the dynamics of cloud droplet coalescence in which droplet fragmentation is assumed to be absent, that is, the process is described by Eq. 6 in which the third and fourth integrals are absent. He obtained analytic solutions of this abridged version of the PBE for a number of different coalescent kinetics and initial droplet size distributions. For the particular case where the agglomeration kinetic function K_A is independent of droplet size and the dimensionless initial droplet size distribution is represented by $N_{SCini}(V_{SC}) = 4V_{SC}\exp(-2V_{SC})$. Scott showed that the exact solution is given by

$$N_{SC}(\tau_{SC}, V_{SC}) = \frac{8\exp(-2V_{SC})\sinh(V_{SC}\sqrt{\tau_{SC}}/\sqrt{2+\tau_{SC}})}{\sqrt{\tau_{SC}(2+\tau_{SC})^3}}. \tag{15}$$

In his investigation, Scott adopted different time and length scales from the analysis above, subscript SC is used to distinguish his dimensionless variables from the τ, V, and N in Eq. 6. The discrete points in Figure 9a are the initial number concentration density and the lighter continuous curves are the exact solution according to Eq. 15 for the τ_{SC} indicated in the figure caption. These results have been converted into volume fraction $G(X_{SC})$ plotted against $X_{SC} = \log_{10} V_{SC}$ as lighter curves in Figure 9b.

The abridged PBE considered by Scott was solved by MoL with the droplet volume restricted to the finite span $10^{-3} = V_{SCmin} \le V_{SC} \le V_{SCmax} = 10^3$. In the exact solution, droplets outside of this finite span are present at very low level, below the resolution limit of the MoL computation, their exclusion in the computation will, therefore, not affect the reliability of the numerical results. These results, for $N_D = 401$, are shown as darker curves in Figures 9a, b. The proximity of the two set of curves attests the accuracy of the MoL results. Because of the nature of the N_{SC} and G, the small difference between the numerical results and the exact solution shows up more clearly in Figure 9a for small τ_{SC} and in Figure 9b for large τ_{SC}. The difference between the computed results and the exact solution is closely related to droplet volume preservation as measured by M_F. This has deteriorated from > 0.9975 at $\tau_{SC} = 4$ to 0.9713 at $\tau_{SC} = 40$. As expected volume preservation, and hence the small difference between the computed results and the exact solution, depends on the number of discretization points. Improvement can be achieved by increasing N_D but at the expense of greatly increased computing time particularly for N_D greater than about 401.

Following the comparison proposed by Kumar and Ramkrishna,[15] the PSD curves in Figure 9a have been replotted with N_{SC} now also in logarithmic scale. This is shown in Figure 9c. This plot shows the agreement between the exact solution and the computed results even when N_{SC} is as small as 10^{-20}. This close agreement should be compared against that reported by Kumar and Ramkrishna.[15] The vast improvement shown by Figure 9c is attributed to the uniformly distributed discretization points in the logarithmic variable $X_{SC} = \log_{10} V_{SC}$ in the present implementation of MoL.

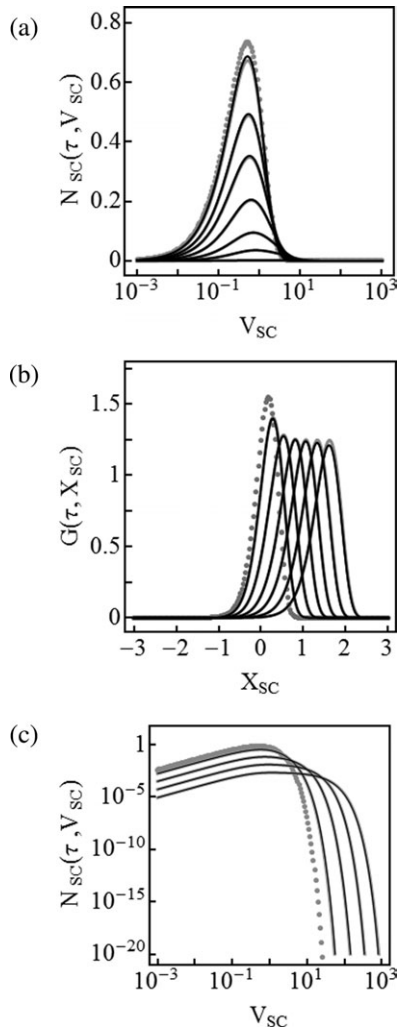

Figure 9. Initial condition and PSD curves of droplet coalescence.

Plotted as $N_{SC}(\tau_{SC}\ V_{SC})$ in (a) and (c) and as $G(\tau_{SC}, X)$ in (b). Discrete points are the initial condition. Dark continuous curves are numerical results of MoL computation and lighter curves are the exact solution based on Eq. 15. τ_{SC} = 0.1, 0.5, 1, 2, 4, 8, 40 (lowest) in (a) τ_{SC} = 0.5, 2, 5, 10, 20, 40 (rightmost) in (b) and τ_{SC} = 1, 5, 15, 40 (rightmost) in (c).

Comparison against an exact solution of the full PBE

Patil and Andrews[16] and subsequently Lage[17] investigated a special case of flocculation in which the composite flocculation kinetics assumed by these authors can be simplified to $k_A(v_s, v_l) = k_F(v_r, v_p) = 1$. One of the dimensionless initial PSDs investigated by these authors is shown as discrete points in Figure 10 described by the function $N_{PAini}(V_{PA}) = 4V_{PA}\exp(-2V_{PA})$ for $0 \le V_{PA} \le \infty$. As in the previous example, subscript PA is used to distinguish the dimensionless variables introduced by Patil and Andrews.[16] They are related to the physical variables by $V_{PA} \equiv v(t)m_Z(0)/m_F$, $\tau_{PA} \equiv k_A m_Z(0)t$ and $N_{PA}(\tau_{PA}, V_{PA}) \equiv n(t, v)m_F/m_Z(0)^2$. For this combination of initial condition and simple constant kinetics, these authors obtained a closed-form solution for the evolving PSD $N_{PA}(\tau_{PA}, V_{PA})$ for $\tau_{PA} > 0$ and $0 \le V_{PA} \le \infty$. Typical

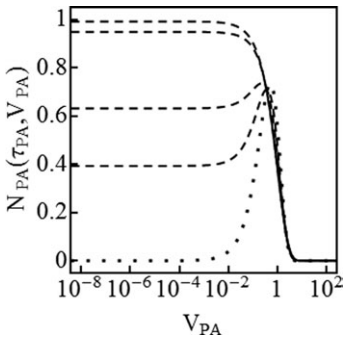

Figure 10. Initial condition and exact solution of Patil and Andrews[16] plotted as number concentration density function.

Discrete points are the initial condition. Broken curves are the exact solution $N_{PA}(\tau_{PA}, V_{PA})$ for $0 \leq \tau_{PA} < \infty$ and $\tau_{PA} = 0.5$, 1, 3, and 5 (top most).

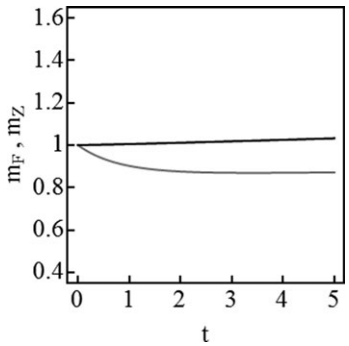

Figure 12. First (m_F) and zeroth (m_Z) moment of $n(t, v)$ for the solution in Figure 11.

Darker curve is for m_F showing a deviation from unity by ~3% at $t = 5$. The lighter curve is $m_Z(t)$ showing reduction of total number of particles.

examples of their exact PSD curves, for $\tau_{PA} = 0.5$, 1, 3, 5, are shown as broken curves in Figure 10. The curve at $\tau_{PA} = 5$ is essentially the equilibrium PSD. A special property of this exact solution is that the zero moment as well as the first moment remains constant at unity, that is, $m_Z(\tau_{PA}) = m_F = 1$.[16] As a consequence, the dimensionless variables τ_{PA}, V_{PA}, and $N_{PA}(\tau_{PA}, V_{PA})$ of Patil and Andrews are numerically identical to the dimensional variables t, v, and $n(t, v)$, respectively. The dimensionless moments $M_Z(\tau_{PA})$ and M_F are also numerically identical with their dimensional analogues.

The subsection of the initial PSD in Figure 10 between $10^{-6} \leq V_{PA} \leq 100$ has been converted into the equivalent $n_{ini}(v)$ and shown as discrete points in Figure 11. With this finite-span initial PSD and $k_A = k_F = 1$, the numerical PSDs given by Eq. 12, after being converted back to dimensional form, are plotted in Figure 11 for $t = 0.5$, 1, 3, 5, where $t = 5$ is again essentially the equilibrium size distribution. As in the previous examples, there is a gradual accumulation of error as equilibrium is approached. This can be seen by plotting the first moment m_F as a function of t (see Figure 12). This is for $N_D = 1001$ and the maximum deviation of m_F from unity is 3%. The corresponding zeroth moment $m_Z(t)$ is also shown in Figure 12. Unlike its analogue for the exact solution, this does not remain constant at unity but decreases with time. Physically, this means that with the restricted particle size between $10^{-6} \leq v \leq 100$, unlike the case of infinite spread, the decrease in the number of particles as a consequence of aggregation is not balanced exactly by the number of particles generated by fragmentation. See further discussion below.

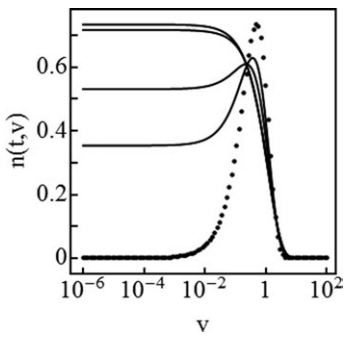

Figure 11. Initial condition and numerical solution plotted as $n(t, v)$ for $k_A = k_F = 1$.

Discrete points are the initial condition. Continuous curves are $n(t, v)$ for $10^{-6} \leq v < 10^{2}$ and $t = 0.5$, 1, 3, and 5 (top most).

The exact and numerical solutions in Figures 10 and 11 exhibit the same general features. For example, both solutions show that, as the PSD evolves, $n(t, v)$ for small v increases from nearly zero to a significant level. Furthermore for $v < 10^{-3}$ (approx.), at any given t, this level is independent of v. However, there is a significant difference in this constant level for the two solutions. This, besides $m_Z(t)$, is another significant difference between the two solutions. As already noted, the exact solution is for infinite spread in particle size, whereas the numerical solution is for a finite span of particle size. The two solutions are solutions to two physically distinct problems and hence their differences.

A more careful comparison between the PSDs in Figures 10 and 11 will have to allow for the difference in zeroth moment. From its definition, it is noted that $N_{PA}(\tau_{PA}, V_{PA})$, as defined by Patil and Andrews, can be viewed as the product of two terms, viz. $[n(t, v)/m_Z(0)] \times [m_F/m_Z(0)]$. The first term can be identified as the number of size v particles as a fraction of the total number of particles at any time t. The second term gives the number-average volume of the particles, which is independent of t for the exact solution. As $m_Z(t)$ is not constant for the numerical solution, its analogue of these two terms are $[n(t, v)/m_Z(t)]$ and $[m_F/m_Z(t)]$, respectively. This led immediately to a modified $N_{PA}(\tau_{PA}, V_{PA})$ for the numerical solution given by $N_{PAmod}(\tau_{PA}, V_{PA}) = n(t, v)m_F/[m_Z(t)]^2$. Figure 13 shows the $N_{PAmod}(\tau_{PA}, V_{PA})$ based on the numerical $n(t, v)$ in Figure 11. The exact $N_{PA}(\tau_{PA}, V_{PA})$ from Figure 10 is also shown on the same plot as lighter points and curves. These two sets of curves are now in close agreement. The remaining difference is that $N_{PAmod}(\tau_{PA}, V_{PA})$ does not extend below $v = 10^{-6}$ or above 100.

Discussion

The main difficulty in solving the PBE of flocculation numerically is the large spread of particle volume—from 6 to 9 or more decades. Ensuring that the discretized PBE provides adequate resolution over the entire size range and over the time span of interest is essential to the success of any solution technique of this integro-differential equation. In the present investigation, this has been achieved by using discretization points that are uniformly spaced in the $\log_{10} V$ space. Typically, each decade of $\log_{10} V$ is divided into 80–110 uniformly spaced grid points. The introduction of the logarithmic-independent variable can be regarded a new development but it can also be viewed

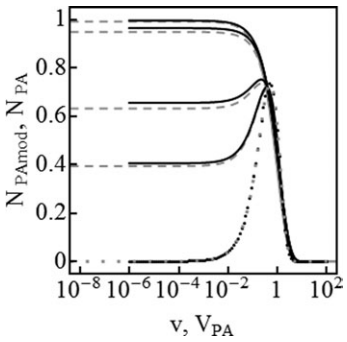

Figure 13. Comparison of exact and numerical solutions.

Lighter points and curves are the exact results $N_{PA}(\tau_{PA}, V_{PA})$ from Figure 10. The darker points and curves are $N_{PAmod}(t, v)$ as defined in the text. $N_{PAmod}(t, v)$ is only valid for the finite range plotted. $\tau_{PA} = t =$ 0.5, 1, 3, and 5 (top most).

as an extension of the geometrically spaced discretization scheme introduced by Batterham et al.[18] and further developed by Hounslow et al.[19] Their discretization scheme in which the step size is doubled from one discretization point to the next can be viewed as a uniform discretization scheme in the transformed-independent variable $\log_2 V$ space. Kumar and Ramkrishna[15] further extended this approach by discretizing the independent variable V so that consecutive discretization points V_i and V_{i+1} are related by $V_{i+1} = \beta V_i$ where β is a positive number between 1.25 and 2. This can be regarded as a uniform discretization scheme in the transformed variable $\log_\beta V$. By reducing β, these authors were able to improve the performance of their discretization scheme. Although geometric discretization of V has improved the numerical representation of the PBE for small V, it has also resulted in unavoidable deterioration in the representation at large V even for β as small as 1.25. Uniform subdivision of $X = \log_\beta V$ with $\beta = 10$ can be regarded as a simple way of remedying the shortcomings of uniform discretization and geometric discretization of V. The logarithmic variable X ensures that the PBE remains well represented at small V and the subdivision of X keeps the deterioration at large V in check.

The improved performance observed in the present discretization scheme immediately suggests that when dealing with the flocculation of submicron particles, where the particle volume may spread over 12 or more decades, the transformed variable $\log_\beta V$, with $\beta = 50$ or 100, may be a possible candidate as the new independent variable. An appropriate combination of β and N_D will help to keep down the number of discretization points and at the same time maintain adequate numerical resolution over the entire enlarged span of particle volume.

All the results reported above were obtained using a standard 2.2 GHz laptop computer with 8 GB RAM. Typically, the computing time required is around 10 min for $N_D = 601$ to over 60 min when $N_D = 1001$. Over 95% of the time was consumed by the integration of the large set of first-order ODEs using standard Runge–Kutta type integration routine with automatic step size adjustment as implemented in most commercial scientific computing software. No attempts have been made to modify or otherwise speed up the routine. For the commercial software used in the present investigation, the maximum RAM used varied from under 2 GB to just over 6 GB. Although this computing hardware requirement is not insignificant, it can be met by current generation of laptops operating under the recently released Windows operating system. Very substantial reduction in RAM requirement and order of magnitude saving in computing time can no doubt be achieved if specially developed software is used to perform the same task. This is not the objective of the present investigation.

The reliability of all the results reported above has been checked by monitoring the first moment M_F of the PSD as it evolves. As already noted, the maximum deviation of the dimensionless M_F from unity was kept below 10% by adjusting N_D. This was in fact the criterion for setting N_D. Numerical experimentation revealed that when only the two fragmentation terms on the RHS of Eq. 12 were included in the PBE only a relatively low N_D was required to ensure that M_F remains within 1% of unity. A much higher N_D was needed to achieve the same degree of accuracy in the case of aggregation and also when both the fragmentation and aggregation terms are included. This is attributed to the nonlinearity introduced by the two aggregation terms. It was also observed that as the flocculation process approaches the equilibrium state, M_F begins to show signs of deterioration. This is understandable as equilibrium is approached, the positive contribution from terms 1 and 3 on the RHS of Eq. 12 will be closely balanced by the negative contribution from terms 2 and 4 leading to increased relative error in the temporal derivative on the lefthand side (LHS). Attempts to compare the PSDs generated by Eq. 12 with some of the computed PSD curves in the literature has not been easy as very often the published results do not report the associated M_F explicitly. It is estimated the M_F of some of these results may have a deviation as large as 15–25%. As the shape of PSD curves, especially those close to equilibrium, is greatly affected by the error in M_F, this makes comparison problematical.

Many investigators treat the kinetics of aggregation and fragmentation as the product of two or more factors, such as collision frequency, collision efficiency, and product distribution function. Each of these factors is in turn a function of the size of the participating particles. Describing these kinetics by the two general functions such as those in Eqs. 2 and 4 may appear, at first glance, to be an over simplification. This is in fact not the case as the products of composite kinetics can be combined and, after nondimensionalization, be identified with the general functions $K_A(V_s, V_t)$ and $K_F(V_r, V_p)$ in Eqs. 7 and 8. As the MoL technique is independent of the functional form of these kinetic functions, it is equally applicable to many of the composite kinetic models reported in the literature.

Results have been presented for a small number of plausible kinetics. It is not the aim of the present investigation to determine the kinetic functions that fits a particular set of empirical PSD. Yeow et al.[3] pointed out that determination of the fragmentation kinetics that best describes a given set of macromolecule disintegration data is an inverse problem and asserted that this requires an entirely different approach and solution technique from that of solving a PBE numerically.[20] This remark is equally valid in the determination of the aggregation and fragmentation kinetics that best describes a given set of flocculation data. The inverse problem in this case is even more complicated as it now involves the determination of two instead of just a single kinetic function. The numerical procedure described here for solving the PBE of flocculation is, in fact, a prerequisite in any meaningful solution of the inverse problem of flocculation.

In the investigation of thermal disintegration of macromolecules, it was observed that the use of off-the-shelf commercial scientific computing software to integrate the ODEs generated

by MoL is a labor-saving way of solving the PBE. In flocculation, the complications brought about by the introduction of the logarithmic-independent variable $X = \log_{10}V$ may have increased slightly the programming effort required but that has certainly not altered this observation.

Conclusions

For suspensions with particle volume V that spans more than 6 decades, the use of a uniform grid in V does not lead to a workable discretized PBE of flocculation. On the other hand, a grid that is uniform in the transformed variable $X = \log_{10} V$ provides a satisfactory basis to discretize the PBE. This together with the MoL converts the PBE from an integro-differential equation into a large set of first-order ODEs. These equations, for different assumed kinetics, can be solved with minimal programming effort using standard ODE solver found in commercial scientific computing software. Reliability of the numerical solutions has been verified by monitoring particulate volume preservation over the entire flocculation process.

Notation

a, b = parameters in dimensionless aggregation kinetic function equation 7
g, h = parameters in dimensionless fragmentation kinetic function equation 8
G = particulate volume fraction density function
k_A = aggregating kinetic function constant, $m^3\ s^{-1}$
k_F = fragmenting kinetic function, $m^{-3}\ s^{-1}$
K_F = dimensionless fragmentation kinetic function = k_F/k_{Fmax}
K_A = dimensionless aggregating kinetic function = $k_A m_F/(v_{max}{}^2 k_{Fmax})$
m_F = first moment of $n(t, v)$ = volume of particulates per unit volume
M_F = dimensionless first moment
m_Z = zero moment of $n(t, v)$ = number of particles per unit volume, m^{-3}
n = number concentration density function, m^{-6}
N = dimensionless number concentration density function = $(v_{max})^2\ n/m_F$
N_D = number of discretization points
N_{PA} = $n(t, v)m_F/m_Z(0)^2$
N_{PAmod} = modified $N_{PA} = n(t, v)m_F/[m_Z(t)]^2$
r_A = aggregation rate, $m^{-9}\ s^{-1}$
r_F = fragmentation rate, $m^{-9}\ s^{-1}$
t = time, s
v = particle size, m^3
v_p, v_q = size of particles formed by fragmentation, m^3
v_r = size fragmenting particle, m^3
v_s, v_t = size of aggregating particles size, m^3
v_u = size of particle formed by aggregation, m^3
V = dimensionless particle size, v/v_{max}
V_{SC} = dimensionless particle size as defined by Scott[14]
V_{PA} = $v(t)m_Z(0)/m_F$
X = $\log_{10} V$
X_{SC} = $\log_{10} V_{SC}$
ΔX = discretization step size, $(X_{max} - X_{min})/(N_D - 1)$

Greek letters

α_{is}, β_{it}, χ_{ir}, γ_{ip} = numerical coefficients arising from quadrature by trapezoidal rule
σ = parameters in dimensionless fragmentation kinetic function equation 8
β = geometrical factor of Kumar and Ramkrishna[15] = V_{i+1}/V_i
τ_{SC} = dimensionless time as defined by Scott[14]
τ_{PA} = $k_A m_Z(0)t$
λ, η = parameters in dimensionless aggregation kinetic function equation 7
τ = dimensionless time = $t \times v_{max} k_{Fmax}$
κ_A = parameter in dimensionless aggregation kinetic function equation 7

Subscripts

i, j, k, p, q, r, s, t, u = positive integers
ini = initial
max = maximum
min = minimum

Literature Cited

1. Randolph AD, Larson MA. *Theory of Particulate Processes*, 2nd ed. San Diego: Academic Press, 1988.
2. Ramkrishna D. *Population Balances.* Regularization of Inverse Problems. San Diego: Academic Press, 2000.
3. Yeow YL, Guan B, Wu L, Yap T-M, Leong Y-K. Obtaining the evolving concentration distribution curves during binary disintegration of macromolecules. *AIChE J*. 2008;54:2699–2706.
4. Thomas DN, Judd SJ, Fawcett N. Flocculation modelling: a review. *Water Res*. 1999;33:1592–1592.
5. Han B, Akeprathumchai S, Wickramasinghe SR, Qian X. Flocculation of biological cells: experiment vs. theory. *AIChE J*. 2003;49: 1687–1701.
6. Ding A, Hounslow MJ, Biggs CA. Population balance modelling of activated sludge flocculation: investigating the size dependence of aggregation, breakage and collision efficiency. *Chem Eng Sci*. 2006;61:63–74.
7. Madras G, Kumar S, Chattopadhyay S. Continuous distribution kinetics for ultrasonic degradation of polymers. *Polym Degrad Stabil*. 2000;69:73–78.
8. Sommer M, Stenger F, Peukert W, Wagner NJ. Agglomeration and breakage of nanoparticles in stirred media mills—a comparison of different methods and models. *Chem Eng Sci*. 2006;61:135–148.
9. Tourbin M, Frances C. Experimental characterization and population balance modelling of the dense silica suspensions aggregation process. *Chem Eng Sci*. 2006;63:5239–5251.
10. Biggs CA, Lant PA. Modelling activated sludge flocculation using population balances. *Powder Technol*. 2002;124:201–211.
11. Brunner H. *Numerical solution of initial-value problems for integro-differential equations*. In: Griffiths DF, Watson GA, editors. *Numerical Analysis 1987, Pitman Research Notes in Mathematics*, vol.170. London: Longmans, 1989:18–38.
12. Press WH, Teukolsky SA, Vetterling WT, Flannery BP. *Numerical Recipes*, 4th ed. Cambridge: Cambridge University Press, 2007.
13. Schiesser WE. *The Numerical Method of Lines*. San Diego: Academic Press, 1991.
14. Scott WT. Analytic studies of cloud droplet coalescence I. *J Atmos Sci*. 1968;25:54–65.
15. Kumar S, Ramkrishna D. On the solution to population balance equations by discretization—I. A fixed pivot technique. *Chem Eng Sci*. 1996;51:1311–1332.
16. Patil DP, Andrews JRG. An analytical solution to continuous population balance model describing floc coalescence and breakage—a special case. *Chem Eng Sci*. 1997;53:599–601.
17. Lage PLC. Comments on the "An analytical solution to the population balance equation with coalescence and breakage—the special case with constant number of particles" by DP Patil and JRG. Andrews [Chem Eng Sci 53: 599–601]. *Chem Eng Sci*. 2002;57:4253–4254.
18. Batterham RJ, Hall JS, Barton G. Pelletizing kinetics and simulation of full-scale balling circuits. In: Molerus O, Hufnagel W, editors. *Proceedings of the Third International Symposium on Agglomeration*, Nürnberg, W. Germany, 1981:A136–A151.
19. Hounslow MJ, Ryall RL, Marshall VR. A discretized population balance for nucleation, growth and aggregation. *AIChE J*. 1988;34:1821–1832.
20. Engl HW, Hanke M, Neubauer A. *Regularization of Inverse Problems*. Dordrecht: Kluwer Academic, 2000.

Manuscript received Jun. 24, 2011, revision received Sept. 15, 2011, and final revision received Nov. 22, 2011.